Prediction of bubble growth and size distribution in polymer foaming based on a new heterogeneous nucleation model

James J. Feng[a)]

The Levich Institute for Physicochemical Hydrodynamics, City College of the City University of New York, New York, New York 10031

Christopher A. Bertelo

ATOFINA Chemicals, Inc., 900 First Avenue, P.O. Box 61536, King of Prussia, Pennsylvania 19406

(Received 20 August 2003; final revision received 26 November 2003)

Synopsis

The cell size distribution in a thermoplastic foam to a large extent determines its mechanical and thermal properties. It is difficult to predict because of the many physical processes involved, each affected in turn by an array of factors and parameters. The two most important processes are bubble nucleation and diffusion-driven bubble growth. Neither has been thoroughly understood despite intensive and long-standing research efforts. In this work, we consider foaming by a physical blowing agent dissolved in a polymer melt that contains particulate nucleating agents. We propose a nucleation model based on the concept that heterogeneous nucleation originates from pre-existing microvoids on the solid particles. The nucleation rate is determined by a bubble detachment time. Once nucleated, the bubbles grow as the dissolved gas diffuses through the polymer melt into the bubbles, a process that couples mass and momentum transport. By using the Oldroyd-B constitutive equation, we explore the role of melt viscoelasticity in this process. Finally, we integrate the nucleation and growth models to predict the evolution of the bubble size distribution. A cell model is employed to simulate the effects of neighboring bubbles and the depletion of blowing agents. The latter also causes the nucleation rate to decline once growth of older bubbles is underway. Using the physical and operating parameters of a recent foam extrusion experiment, we are able to predict a cell size distribution in reasonable agreement with measurements. © *2004 The Society of Rheology.* [DOI: 10.1122/1.1645518]

I. INTRODUCTION

The foaming of a polymer melt is an important process because of its practical and scientific values. Whether the product is used for its mechanical strength or thermal insulation, the cell size distribution (CSD) is a critical determinant for the quality of the product. Despite long-standing interest and research effort, the problem is far from being fully resolved. Many processes affect the final CSD of a foam, including bubble nucleation, growth, deformation, and possibly coalescence and burst. Each of these in turn depends on a host of factors, such as melt rheology, solubility of the blowing agent,

[a)]Current address: Department of Chemical and Biological Engineering and Department of Mathematics, University of British Columbia, Vancouver BC V6T 1Z4, Canada; electronic mail: jfeng@chml.ubc.ca

temperature, pressure, and the use of nucleating agents. The literature is chiefly concerned with the first two stages of foaming: nucleation and growth. The former provides the initial condition for the latter. The stability of a foam against collapse is a more difficult problem, and appears to have received relatively few studies.

Nucleation is a well-studied problem, playing an essential role in a variety of processes ranging from boiling to crystal growth. The classical nucleation theory is based on the Gibbs free energy required for creating a void in a liquid, and centers around the concept of the *critical bubble* in mechanical and thermodynamic equilibrium with the surrounding liquid (Cole 1974; Hodgson 1984). Bubbles larger than the critical bubble grow further while smaller ones dissolve. Despite its success in problems such as boiling of low-molecular-weight liquids, the classical theory does not apply to polymer foaming. Calculations have shown that when applied to polymers under typical foaming conditions, the rate of homogeneous nucleation is negligible (Han and Han 1990b; Saunders 1991). Numerous adaptations of the classical theory have been proposed. The free energy has been modified to account for changes in the polymer free-volume (Colton and Suh 1987), the presence of solid surfaces (Cole 1974; Colton and Suh 1987), supersaturation of the blowing agent (Han and Han 1990b), polymer-solvent interactions in foaming a solution (Han and Han 1990b), and surface tension reduction due to dissolved gas (Lee and Flumerfelt 1996). In addition, shear-induced nucleation has received much attention, with the general conclusion that shear increases the nucleation rate (e.g., Lee 2000; Chen *et al.* 2002; Guo and Peng 2003). Yarin *et al.* (1999) proposed a model based on the intriguing idea of stress-induced secondary nucleation.

From our perspective of studying the final CSD, these models have three shortcomings. First, they predict a nucleation rate of the critical bubbles at radius R_{cr}. But a critical bubble will neither grow nor shrink. The nucleation models thus fail to provide an initial condition for subsequent bubble growth. Recognizing this problem, Shafi and Flumerfelt (1997) attempted to derive an initial condition that corresponds to the ''upper bound of the critical region,'' where thermal fluctuation cannot drive a supercritical bubble to subcritical. Though an interesting idea, its implementation is not straightforward. Shafi and Flumerfelt's (1997) mathematical procedure is incorrect in treating a singular perturbation as a regular one. Second, without a proper bubble growth model, these nucleation models cannot be easily tested against experiments, which invariably measure larger ''grown-up'' bubbles. Thus, the merit of the various new features added to the classic theory is not readily ascertainable. Finally, the picture of critical bubbles spontaneously arising in the bulk is irrelevant to most polymer foaming processes. Nonhomogeneity and impurities are ubiquitous in commercial resins, and nucleating agents are commonly added to promote nucleation in the foaming process (Park *et al.* 1998). The classic theory handles heterogeneous nucleation by simply adding a prefactor in front of the free energy; its effect is insufficient by far to account for the high nucleation rates in reality (Cole 1974).

Thus, the first task of our study is to develop a more realistic nucleation model. We have come to understand that pre-existing microbubbles on the surface of particulate nucleating agents are an important route for nucleation in polymer foaming. These microbubbles are trapped in surface cavities or crevices, and act as the seed for nucleation when the pressure or temperature becomes favorable (Griffith and Wallis 1960; Cole 1974; Ramesh *et al.* 1994a, b). This picture is formulated into a heterogeneous nucleation model to be discussed in the next section. Note that this is unrelated to prior heterogeneous nucleation models that represent the effect of solid surfaces by a reduction in the Gibbs free energy (Colton and Suh 1987; Shafi *et al.* 1997).

In comparison with nucleation, bubble growth is a much better defined problem. There have been studies on diffusion-driven bubble growth in Newtonian, power-law, and viscoelastic melts, with the mass and momentum transfer properly coupled (Ramesh *et al.* 1991; Arefmanesh and Advani 1991; Venerus and Yala 1997; Venerus *et al.* 1998). Bubbles are assumed to remain spherical during growth. Bubble-bubble interaction is accounted for, to a limited extent, by a cell model where the influence of other bubbles is represented by a finite shell of polymer melt. Our interest in the bubble growth model is twofold. First, it is a critical part in our endeavor to predict the CSD of a foam. We need to develop an accurate numerical scheme for computing bubble growth. Second, we wish to delineate clearly the effect of viscoelasticity on bubble growth; this important issue has not been adequately elucidated in the past.

The final task of our study is to integrate the nucleation and growth models into a consistent theory capable of predicting the evolution of the bubble size distribution during foaming. Using parameter values corresponding to a recent foam extrusion experiment (Kieken 2001), we obtain a CSD in reasonable agreement with that measured in the experiment. In this study, we have assumed that the temperature remains constant, as do all the material properties except for the gas density in the bubble. In particular, we neglect changes of melt density and viscosity due to the loss of blowing agent. Furthermore, spatial homogeneity is assumed when calculating the CSD, neglecting any macroscopic spatial gradients related to the geometry of actual processing units. Some of these factors are obviously important in reality, and the simplifications are made to render the problem tractable.

II. NUCLEATION MODEL

It has been long established in the boiling literature that crevices and depressions on solid surfaces harbor microbubbles that will serve as nuclei for boiling (Griffith and Wallis 1960; Cole 1974). In polymer foaming experiments, Tatibouët *et al.* (2002) observed that dissolved gas tends to aggregate on the surface of the nucleating agents, and surmised that such aggregations will become nucleation sites during foaming or degassing. Using electron microscopy, Ramesh *et al.* (1994a) confirmed the existence of microvoids on rubber particles added to polystyrene as nucleating agents. They further proposed a nucleation model from which our nucleation model draws certain elements.

The Ramesh *et al.* (1994a, b) model is based on three key assumptions:

(1) Each particle produces one bubble from its largest microvoid. Bubbles created by smaller voids, if any, are absorbed by the largest one during the onset of bubble growth.
(2) The size of the nucleated bubbles scales with the size of the particle.
(3) There is a minimum size R^* for the bubble to be viable; larger ones grow further while smaller ones disappear.

Much of the effort in Ramesh *et al.* (1994a, b) is devoted to determining the cutoff R^* for a postulated lognormal distribution for the initial bubbles. This procedure appears to suffer from several inconsistencies. The criterion for the survival of the bubble is a force balance between the bubble pressure P_g and resisting forces due to surface tension and elastic stresses. P_g is calculated from a mass conservation by assuming that the gas concentration outside remains uniform and in equilibrium with P_g. This is tantamount to assuming an infinitely large gas diffusivity in the melt. Besides, the elastic stress should be due to the polymer melt surrounding the bubble. Subsequently, however, the stress is computed using the *rubber particle's* modulus since ''the nucleation is considered to be a

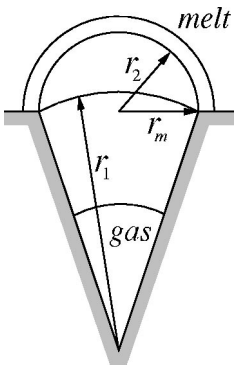

FIG. 1. The nucleation of a bubble from a pre-existing microvoid on the surface of a solid particle.

local event occurring inside the rubber particle.'' Finally, the particles have a lognormal size distribution with the finer particles unable to produce viable bubbles. This cutoff implies that the bubbles should have a ''truncated'' lognormal size distribution instead of the full lognormal assumed by Ramesh *et al.* (1994a).

Our nucleation model adopts their Assumptions 2 and 3, but determines R^* by borrowing the picture of bubble formation on a rough surface in classical boiling theory (Griffith and Wallis 1960; Cole 1974). In this picture, a bubble grows from a dormant vapor microbubble trapped in a surface crevice or depression modeled as a conical cavity (Fig. 1). The pre-existing microbubble is initially saturated with vapor at pressure P_0. When the ambient pressure is reduced abruptly from P_0 to P_a, the microbubble starts to expand toward the mouth. The radius of curvature r increases with bubble volume until the contact line reaches the lip of the cavity, when $r = r_1$ is at a maximum. Then r decreases as the bubble bulges out to form a ''cap.'' When the interface is at the proper contact angle with the *outside* portion of the solid surface, $r = r_2$ is at a minimum. Griffith and Wallis (1960) assumed a contact angle of $\theta = \pi/2$ and thus $r_2 = r_m$, the radius of the mouth of the cavity. Here comes in the classical concept of the critical bubble: If $r_2 \geqslant R_{\rm cr}$, the bubble will grow further and eventually detach. Otherwise it will stay at r_2. The existence of such seed microbubbles and their role in boiling have been well established by experiments (Cole 1974), and the criterion for active nucleation sites $r_m \geqslant R_{\rm cr}$ turns out to be approximately valid over a wide range of contact angles.

In our case, we assume that the radius of the detached bubble R_0, to be used as an initial condition for subsequent growth, is related to the particle size R_p. The exact relationship, however, depends on the detachment process, of which we have no detailed knowledge. Furthermore, because of their tiny size, there is no information on the shape and dimension of the microvoids on filler particles; hence r_m is essentially unknown. We circumvent these two difficulties by making the following *ad hoc* assumption: the initial bubble created by a particle shall have a radius R_0 proportional to the particle radius R_p.

$$R_0 = \epsilon R_p, \tag{1}$$

where the phenomenological coefficient ϵ is to be determined by comparison with experiments.[1] Presumably, ϵ depends on the shape, size, and surface property of the particle and the cavity. These effects can be clarified by measuring R_0 on various well-

[1]If one ignores the cavity and considers the detachment of a gas cap from a smooth sphere, ϵ can be calculated from the contact angle. In our context, however, it is treated as a phenomenological constant.

defined cavities. As will be shown in Sec. IV, however, the predicted CSD is not very sensitive to ϵ over a reasonable range. Based on Eq. (1), the size distribution of the solid nucleating agents is readily transformed into a size distribution for the initial bubbles. Only those with a radius greater than $R_{\rm cr}$ will survive, grow, and contribute to the final CSD.

Another feature of our nucleation model is that we abandon the Assumption 1 of Ramesh *et al.* (1994a) and allow *continuous nucleation* from the same site. Assumption 1 is based on the premise that a larger bubble encounters a lower interfacial tension and grows faster, thereby annexing the smaller bubbles nucleating from the same solid particle. Our simulations show that, for typical processing conditions, the viscoelastic stress in the melt contributes much more resistance to bubble growth than the interfacial tension. Consequently, the growth rate shows only a weak dependence on R_0. More importantly, experiments show the total number of bubbles to be several times more than that of the solid particles (Kieken 2001). These have led us to believe that bubbles are continuously produced by a particle, from one or several active cavities. The rate of production depends on a *detachment time*, which in turn depends on the gas diffusivity and cavity geometry among other factors. The most relevant time scale appears to be the diffusion time $\tau_D = R_0^2/D$, D being the diffusivity of the blowing agent in the melt. Thus, we take the detachment time to be proportional to τ_D. Furthermore, we anticipate the nucleation to slow down in time as bubble growth gradually uses up the dissolved gas in the melt. A similar idea was used in the nucleation model of Shafi *et al.* (1997) to account for simultaneous nucleation and growth. Here we quantify the effect by designating the first bubble produced by a particle the ''primary bubble.'' As the primary bubble grows, a gas concentration c_s representative of the neighborhood, to be defined in Sec. IV in the cell model, decreases in time. Assuming a *linear* dependence of the nucleation rate on c_s, we write the number of secondary bubbles produced by the particle in unit time as

$$Q(R_0,t) = \gamma \frac{D c_s(R_0,t)}{R_0^2}, \tag{2}$$

where γ is to be determined from experimental measurements on the total number of bubbles. Note that γ lumps all the factors that are not explicitly accounted for, including the amount of initially trapped air, the depletion effect of nearby bubbles, and the inhomogeneity of the gas concentration in the neighborhood. The linearity of Eq. (2) in c_s is motivated by scaling arguments based on the governing equations for bubble growth to be presented in the next section. This turns out to underpredict the suppression of nucleation by a declining c_s; we will revisit this point at the end of Sec. IV. We further assume that all secondary bubbles have the same radius R_0 as the primary one, and follow the same growth curve $R = R(R_0, t-t_0)$, where t_0 is the instant of nucleation.

As initial conditions for computing the ensuing bubble growth, we have the bubble radius in Eq. (1). The initial velocity of bubble expansion is taken to be zero. The initial condition for the bubble pressure requires somewhat more involved considerations. Han and Yoo (1981) and Arefmanesh and Advani (1991), among others, have assumed that the initial bubble pressure is equal to the initial vapor pressure

$$P_g(0) = P_0. \tag{3}$$

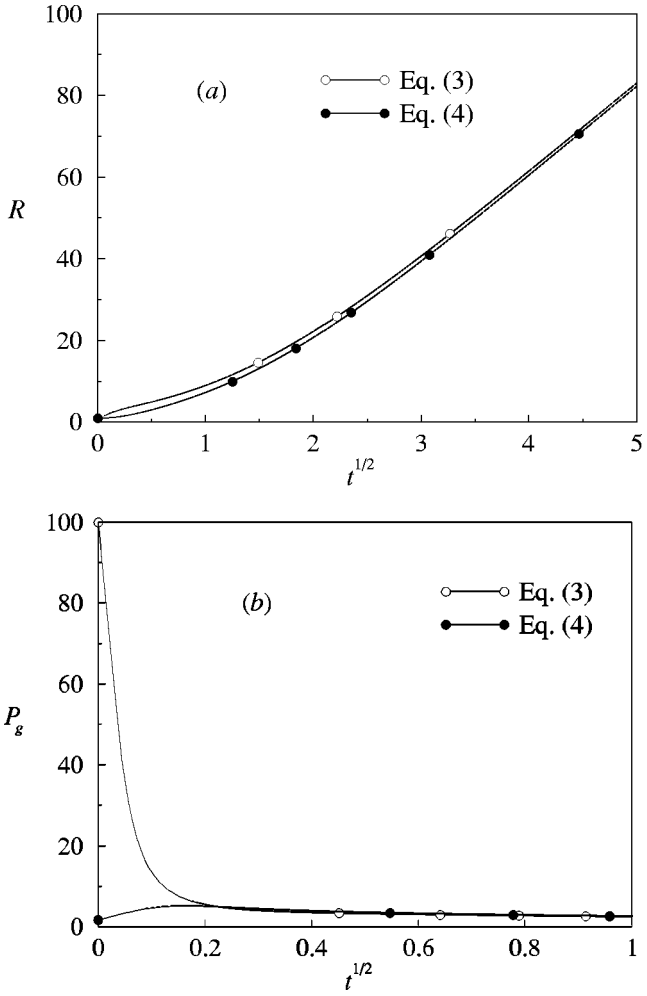

FIG. 2. Effects of the pressure initial condition on subsequent growth as predicted by the model described in Sec. III. The dimensionless parameters, to be defined in that section, have the following values: Pa* = 1, Re = 10^{-6}, Ca = 2.5, $\beta = 0.1$, $k^* = 0.01$, $A^* = 9.9$, and De = 1. (a) Bubble growth as indicated by its radius $R(t)$; (b) evolution of the bubble pressure $P_g(t)$. The nondimensionalization of R, t, and P_g will be given in Sec. III. The abscissa is taken to be $t^{1/2}$ to reflect the diffusion-controlled dynamics at large t (Venerus *et al.* 1998).

This ensures thermodynamic equilibrium for the dissolution of gas at the bubble's surface. Since $R_0 > R_{\rm cr}$, however, the surface tension can no longer withstand P_0, and the bubble will expand with a nonzero acceleration. An alternative is to postulate (Venerus *et al.* 1998)

$$P_g(0) = P_a + \frac{2\sigma}{R_0}, \tag{4}$$

which maintains the force balance, but incurs a discontinuity in the gas concentration at the interface and thus immediate diffusion of gas into the bubble. Our picture for the birth of bubbles in Fig. 1 is a nonequilibrium process. The detachment occurs after the bubble has grown out of the cavity. The internal pressure should have relaxed somewhat from the

initial vapor pressure, yet should still be higher than that in Eq. (4) so further growth is maintained. Thus our nucleation model implies an initial $P_g(0)$ between Eqs. (3) and (4). Numerical experiments show that the influence of $P_g(0)$ is largely limited to the initial moments of bubble growth (Fig. 2); the difference is qualitatively unimportant in later times. We have adopted Eq. (4) in all subsequent calculations since the initial force imbalance due to Eq. (3) causes an unnatural initial acceleration. Incidentally, Blander and Katz (1975) discussed the effect of $P_g(0)$ on the free energy of homogeneous nucleation, with the conclusion that using Eq. (3) or (4) produces a negligible difference in the nucleation rate.

III. DIFFUSION-INDUCED BUBBLE GROWTH

There have been numerous studies of diffusion-induced growth or collapse of bubbles in a fluid. Venerus *et al.* (1998) presented a complete set of equations for bubble growth in an infinite expanse of viscoelastic fluid and examined the various approximations used in the literature. Arefmanesh and Advani (1991) considered the growth of a bubble enclosed in a shell of liquid containing a finite amount of dissolved gas. This ''cell model'' approximates the situation in polymer foaming where the depletion of the blowing agent and proximity of nearby bubbles prevent the bubbles from growing indefinitely. Both articles have reviewed earlier work on the topic. Given this wealth of previous research, we have a twofold purpose in this section. First, we wish to establish the validity and accuracy of our numerical scheme by comparison with previous results. Second, we will shed some light on the effect of viscoelasticity in the bubble growth process. Both serve as preparations for the prediction of CSD to be discussed in the next section.

A. Bubble growth in an unbounded Oldroyd-B fluid

A gaseous blowing agent is dissolved into a polymer melt under high pressure P_0 to saturation concentration $c_0 = kP_0$, where k is Henry's constant. Then the pressure is suddenly reduced to P_a and the blowing agent becomes super-saturated. Nucleation occurs, and a viable bubble proceeds to grow as the dissolved gas diffuses into the bubble. For this process of coupled momentum and mass transfer, we assume constant temperature and a spherical shape for the bubble, and use the same governing equations as in Venerus *et al.* (1998) with the infinitely dilute solute assumption. Melt viscoelasticity is represented by the Oldroyd-B model. Venerus *et al.* (1998) tested the Phan-Thien-Tanner model and found that the more complex rheology has only a minor effect on bubble growth. In dimensional forms, the governing equations are as follows:
(a) Momentum equation:

$$P_g - P_a = \rho\left(R\ddot{R} + \frac{3}{2}\dot{R}^2\right) + \frac{2\sigma}{R} + \frac{4\mu_s\dot{R}}{R} - 2\int_R^\infty \frac{\tau_{rr} - \tau_{\theta\theta}}{r}\,dr, \tag{5}$$

where $P_g(t)$ and $R(t)$ are the instantaneous bubble pressure and radius, σ is surface tension, μ_s is the Newtonian viscosity and τ_{rr} and $\tau_{\theta\theta}$ are the viscoelastic normal stress components. The dot over R indicates time derivative. The terms on the right-hand side represent resistance to bubble growth due, respectively, to inertia, surface tension, viscous, and viscoelastic normal stresses.
(b) Mass balance for gas in the bubble:

$$\frac{d}{dt}(P_g R^3) = 3DAR^2 \left.\frac{\partial c}{\partial r}\right|_{r=R}, \tag{6}$$

where A is a constant for the isothermal ideal gas: $P_g = A\rho_g$, and D is the gas diffusivity in the melt. $c(r,t)$ is the mass concentration of the gas in the melt.
(c) Mass balance for gas in melt:

$$\frac{\partial c}{\partial t} + v_r \frac{\partial c}{\partial r} = \frac{D}{r^2}\frac{\partial}{\partial r}\left(r^2 \frac{\partial c}{\partial r}\right), \tag{7}$$

where $v_r(r,t) = R^2\dot{R}/r^2$ is the radial velocity in the melt.
(d) Oldroyd-B constitutive equations:

$$\tau_{rr} + \lambda\left(\frac{d\tau_{rr}}{dt} + \frac{4R^2\dot{R}}{r^3}\tau_{rr}\right) = -\frac{4\mu_p R^2\dot{R}}{r^3}, \tag{8}$$

$$\tau_{\theta\theta} + \lambda\left(\frac{d\tau_{\theta\theta}}{dt} - \frac{2R^2\dot{R}}{r^3}\tau_{\theta\theta}\right) = \frac{2\mu_p R^2\dot{R}}{r^3}, \tag{9}$$

where λ is the polymer relaxation time and μ_p the polymer viscosity. A biaxial-extensional kinematics has been assumed, with $v_r(r,t) = R^2\dot{R}/r^2$ being the only non-vanishing velocity component. $d/dt = \partial/\partial t + v_r\partial/\partial r$ is the material derivative.

These equations are supplemented by the following initial and boundary conditions:

$$c(r,0) = c_0, \tag{10}$$

$$c(R,t) = kP_g(t), \tag{11}$$

$$c(\infty,t) = c_0, \tag{12}$$

$$R(0) = R_0, \tag{13}$$

$$\dot{R}(0) = 0, \tag{14}$$

$$P_g(0) = P_a + 2\sigma/R_0, \tag{15}$$

$$\tau_{rr}(r,0) = 0, \tag{16}$$

$$\tau_{\theta\theta}(r,0) = 0, \tag{17}$$

where thermodynamic equilibrium is assumed at the bubble surface and Henry's law is applied.

As in Venerus *et al.* (1998), we use R_0 as the length scale and R_0^2/D as the time scale. Pressure and the stresses are scaled by $\mu D/R_0^2$, where $\mu = \mu_s + \mu_p$, and the gas concentration c by its initial value c_0. Then we have the following dimensionless equations (same symbols are used for the variables; some dimensionless groups are indicated by an asterisk):

$$P_g - P_a^* = \mathrm{Re}\left(R\ddot{R} + \frac{3}{2}\dot{R}^2\right) + \frac{2}{\mathrm{Ca}}\frac{1}{R} + \frac{4\beta\dot{R}}{R} - 2\int_R^\infty \frac{\tau_{rr} - \tau_{\theta\theta}}{r}dr, \tag{18}$$

$$\frac{d}{dt}(P_g R^3) = \frac{3}{A^* k^*} R^2 \left.\frac{\partial c}{\partial r}\right|_{r=R}, \tag{19}$$

$$\frac{\partial c}{\partial t} + v\frac{\partial c}{\partial r} = \frac{1}{r^2}\frac{\partial}{\partial r}\left(r^2 \frac{\partial c}{\partial r}\right), \tag{20}$$

$$\tau_{rr} + \mathrm{De}\left(\frac{d\tau_{rr}}{dt} + \frac{4R^2\dot{R}}{r^3}\tau_{rr}\right) = -4(1-\beta)\frac{R^2\dot{R}}{r^3}, \tag{21}$$

$$\tau_{\theta\theta} + \mathrm{De}\left(\frac{d\tau_{\theta\theta}}{dt} - \frac{2R^2\dot{R}}{r^3}\tau_{\theta\theta}\right) = 2(1-\beta)\frac{R^2\dot{R}}{r^3}, \tag{22}$$

with the following initial and boundary conditions:

$$c(r,0) = 1, \tag{23}$$

$$c(R,t) = k^* P_g(t), \tag{24}$$

$$c(\infty,t) = 1, \tag{25}$$

$$R(0) = 1, \tag{26}$$

$$\dot{R}(0) = 0, \tag{27}$$

$$P_g(0) = P_a^* + 2/\mathrm{Ca}, \tag{28}$$

$$\tau_{rr}(r,0) = 0, \tag{29}$$

$$\tau_{\theta\theta}(r,0) = 0, \tag{30}$$

where the dimensionless groups are

$$P_a^* = \frac{P_a R_0^2}{\mu D}, \tag{31}$$

$$\mathrm{Re} = \rho D/\mu, \tag{32}$$

$$\mathrm{Ca} = \frac{\mu D}{\sigma R_0}, \tag{33}$$

$$\beta = \mu_s/\mu, \tag{34}$$

$$k^* = \frac{k\mu D}{c_0 R_0^2}, \tag{35}$$

$$A^* = A/k, \tag{36}$$

$$\mathrm{De} = \lambda D/R_0^2. \tag{37}$$

To solve the governing Eqs. (18)–(22) on the domain $r \in [R,\infty)$, we adopt the coordinate transformation used by Duda and Vrentas (1969) and Venerus *et al.* (1998): $\theta = 1 - \exp[-\alpha(r/R - 1)]$, where the constant α controls the ''compression'' of the spa-

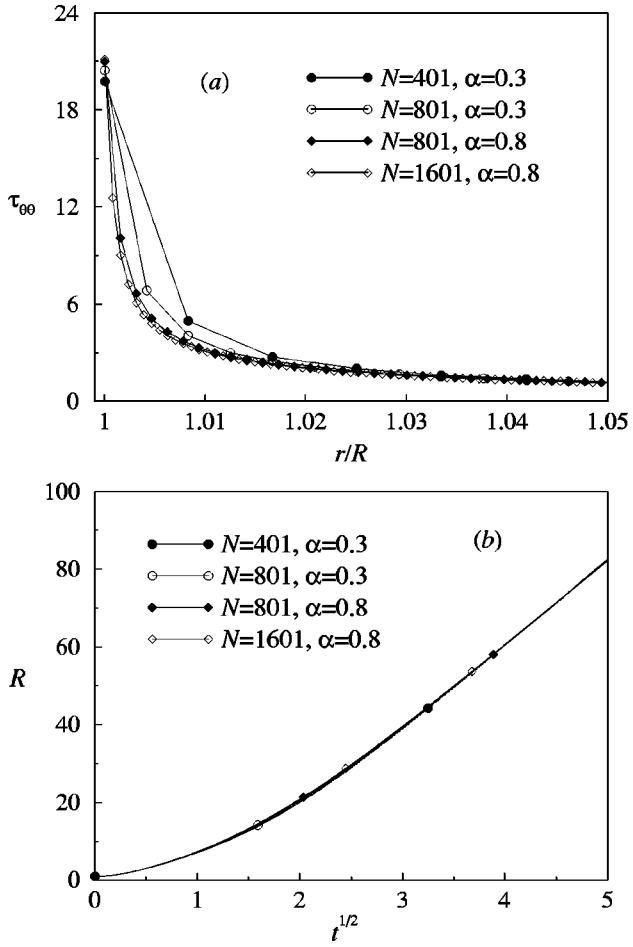

FIG. 3. Mesh refinement for the solution of a bubble growing in a Oldroyd-B fluid. N is the total number of nodes, and α is a parameter in the coordinate transformation (see text). The dimensionless parameters correspond to those used by Venerus *et al.* (1998): $\mathrm{Pa}^* = 1$, $\mathrm{Re} = 10^{-6}$, $\mathrm{Ca} = 2.5$, $\beta = 0.1$, $k^* = 0.01$, $A^* = 9.9$, and $\mathrm{De} = 1$. (a) Resolution of the stress boundary layer at $t = 1.5$; (b) bubble growth is insensitive to how well the stress boundary layer is resolved.

tial coordinate as the domain transforms from $[R,\infty)$ to $[0,1]$. We use a nonuniform grid over the θ-domain with denser grid points at the bubble; the grid size increases by a factor (typically 1.01) along θ between neighboring nodes. The diffusion and constitutive Eqs. (18)–(20) are then discretized on the grid, resulting in a system of coupled ordinary differential equations (in time) for R, P_g and the values of c, τ_{rr}, and $\tau_{\theta\theta}$ on each grid point. These have been solved by two different methods: a fourth-order Runge-Kutta explicit scheme and an implicit scheme using Newton iteration and the Woodbury algorithm for fast matrix inversion (Press *et al.* 1992). The results are nearly identical. In terms of spatial resolution, $\tau_{\theta\theta}$ is the most demanding. Shortly after the bubble starts to expand, $\tau_{\theta\theta}$ develops a very steep boundary layer outside the bubble, which requires a much more refined grid than is sufficient to resolve the $c(r)$ profile. Figure 3(a) illustrates the resolution of the $\tau_{\theta\theta}$ boundary layer on four different meshes at $t = 1.5$, when $\tau_{\theta\theta}(R)$ peaks in time. For the explicit solver, upwinding is necessary to prevent oscillations in the $\tau_{\theta\theta}(r)$ profile. Remarkably, poor resolution of $\tau_{\theta\theta}$ on a coarser mesh has

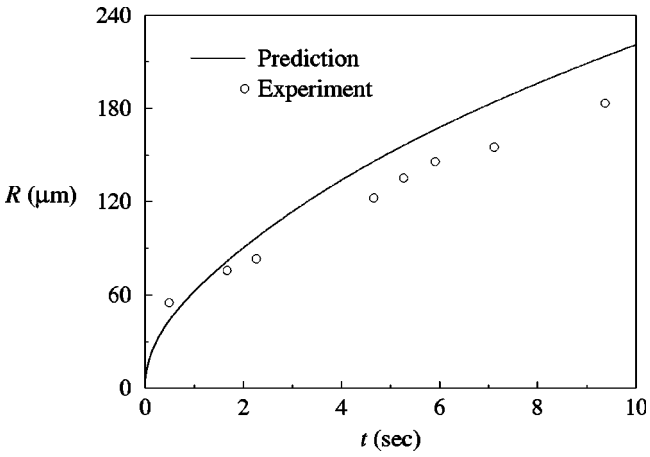

FIG. 4. Comparison between model prediction of $R(t)$ and experimental measurement of Han and Yoo (1981). The dimensionless parameters are: $\mathrm{Pa}^* = 0.04605$, $\mathrm{Re} = 1.21\times10^{-10}$, $\mathrm{Ca} = 78.57$, $\beta = 0$, $k^* = 4.686$, $A^* = 2.983$, and $\mathrm{De} = 495.0$.

little effect on the growth of the bubble $R(t)$ [Fig. 3(b)]. This is evidently because the boundary layer is too narrow to contribute much to the stress integral in Eq. (18). Later in time, the stress boundary layer subsides and its resolution becomes easier. The gas concentration profile $c(r)$ is well resolved by even the coarsest grid ($N = 401$, $\alpha = 0.3$) over the entire time. Subsequent computations are mostly done on an intermediate grid with $N = 801$ and $\alpha = 0.8$.

To further benchmark our numerical method, we compared our solutions to previous numerical and experimental results. For diffusion-controlled and diffusion-induced bubble growth in a Newtonian fluid ($\beta = 1$), our solutions are indistinguishable from those in Duda and Vrentas (1969) and Venerus and Yala (1997). For Oldroyd-B fluids, our results are in good agreement with those of Venerus *et al.* (1998). Furthermore, we compared our predictions with the experimental measurements of Han and Yoo (1981). These authors recorded the growth of bubbles during injection molding of a polystyrene foam with CO_2 as the blowing agent. The physical and operating parameters in the experiment are converted into our dimensionless parameters, and the model predicts a bubble radius in reasonable agreement with the measurements (Fig. 4). That the bubble grows more slowly in the experiment is probably because the foam is a multibubble system enclosed in a cavity. The bounding walls and the depletion of blowing agent in the melt by neighboring bubbles both tend to hamper the growth of the bubbles.

B. Bubble growth in a shell of Oldroyd-B fluid

The cell model, with a single bubble growing within a shell of polymer melt containing a finite amount of dissolved gas, is motivated by the fact that a multitude of bubbles grow in close proximity in actual foaming. Growth will be arrested once the dissolved gas in the melt is exhausted. The behavior of a single cell was studied by Amon and Denson (1984), Arefmanesh and Advani (1991), and Ramesh *et al.* (1991). Amon and Denson (1986), Arefmanesh *et al.* (1990), and Koopmans *et al.* (2000) have attempted to predict macroscopic flow fields during foam molding and extrusion on the basis of the local cell model. Our interest in the cell model derives from the fact that to predict the

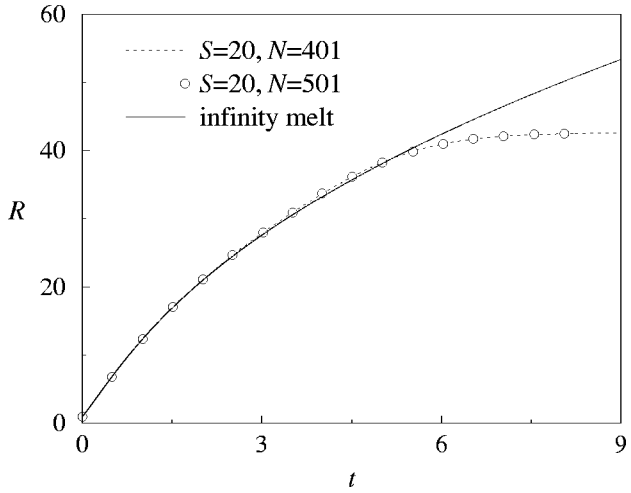

FIG. 5. Bubble growth in a shell of Oldroyd-B fluid. The shell has an initial radius $S = 20R_0$, R_0 being the initial bubble radius. The dimensionless parameters are: Pa* = 1, Re = 10^{-6}, Ca = 2.5, $\beta = 0.1$, $k^* = 0.01$, $A^* = 9.9$, and De = 100. Because of the nonuniformity of the mesh, increasing N from 401 to 501 reduces the minimum grid size at the bubble by nearly a factor of 3. The growth curve in an infinite sea of melt is also shown for comparison.

cell size distribution, some account of cell-cell interaction has to be incorporated. Besides, the depletion of blowing agent enters our nucleation model [Eq. (2)] as well.

The bubble growth model discussed in the last subsection is easily adapted to the cell model by replacing the Dirichlet condition $c(\infty,t) = 1$ [Eq. (25)] by a Neumann condition

$$\left.\frac{\partial c}{\partial r}\right|_{r = S(t)} = 0, \tag{38}$$

where $S(t)$ indicates the expanding outer boundary of the shell. To track the time-dependent computational domain, a Lagrangian coordinate is advantageous (Arefmanesh and Advani 1991)

$$y = r^3 - R(t)^3. \tag{39}$$

In terms of y, the computational domain is once again time-independent. An added benefit is that the material derivatives in the gas diffusion equation and constitutive equations are computed directly and no spatial differentiation or upwinding is necessary. A new difficulty arises, however, from the y-mesh. As the bubble and shell expand, the y-grid is carried along, resulting in a squeezing of the corresponding mesh in the physical domain. This causes the time step to drop rapidly in an explicit scheme. We have circumvented this difficulty by periodically coarsening the y-grid for the gas-diffusion equation [Eq. (20)]. The constitutive equations contain no spatial derivative and require no coarsening; in fact, a fine mesh is necessary to resolve the $\tau_{\theta\theta}$ boundary layer at the bubble. As an example, Fig. 5 plots the growth curve of a bubble in a shell computed on two different meshes. Convergence with mesh refinement is evident. Initially, the shell-to-bubble radius ratio is $S/R_0 = 20$. At the end, this ratio has dropped to a mere 1.033, indicating the severe squeeze that the melt was subjected to. Also shown in Fig. 5 is the growth curve of a bubble in an infinite sea of melt under the same conditions. For some

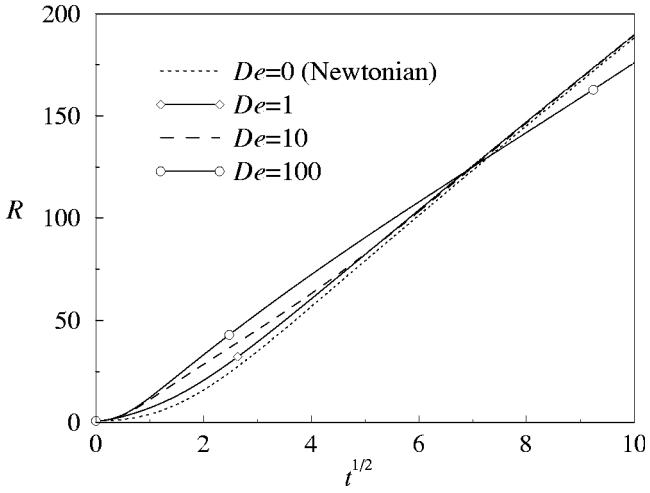

FIG. 6. Effects of De on bubble growth in an infinite expanse of Oldroyd-B melt. All other parameters are the same as in Fig. 5.

intermediate period ($2 < t < 5$), the bubble in the shell grows faster than that in an infinite melt. This is because the stress profiles have developed by then, and the additional contribution from the far-away melt to the stress integral [Eq. (18)] hampers the growth in an infinite melt. Later, the trend is reversed because the finite amount of blowing agent dissolved in the shell is being exhausted. The bubble in the shell eventually approaches an equilibrium size.

C. Effects of viscoelasticity

With the model and numerical method properly validated, we turn now to the physical question of the effect of melt viscoelasticity on bubble growth. There seems to be a consensus in the literature that viscoelasticity *enhances* bubble growth, for a single bubble in an infinite sea of melt (Street 1968; Han and Yoo 1981; Venerus *et al.* 1998) as well as in the cell model (Arefmanesh and Advani 1991; Ramesh *et al.* 1991). Yet, this contradicts the intuition informed by experiments that increasing the ''melt strength,'' by way of increasing the molecular weight (MW) or adding a high-MW foaming aid, produces smaller and more uniform bubbles (Sandler *et al.* 2000; Azimipour 2002).

There are in fact two layers to this question. The first is the effect of the Deborah number De (or dimensionless relaxation time) within the theoretical framework of a certain constitutive equation. The second is the relevance of this effect to the actual process of polymer foaming. To address the first, we systematically varied De using the Oldroyd-B model while keeping the other dimensionless parameters unchanged. This amounts to changing the relaxation time of the polymer melt alone. The results, shown in Fig. 6, reveal an interesting crossover. For a small De, a bubble grows faster than in a Newtonian melt with the same viscosity. With increasing De, the growth is faster initially, but is *suppressed* at some later time and falls below the Newtonian curve. Furthermore, the larger De is, the later the suppression occurs.

Viscoelasticity affects bubble growth via the normal stress integral in the momentum equation [Eq. (18)]. The expansion of the bubble subjects the melt to a biaxial extension, producing a positive $\tau_{\theta\theta}$ and a negative τ_{rr}, both opposing the bubble growth. The tensile stress $\tau_{\theta\theta}$ is greater than the compressive stress $|\tau_{rr}|$ by over two orders of

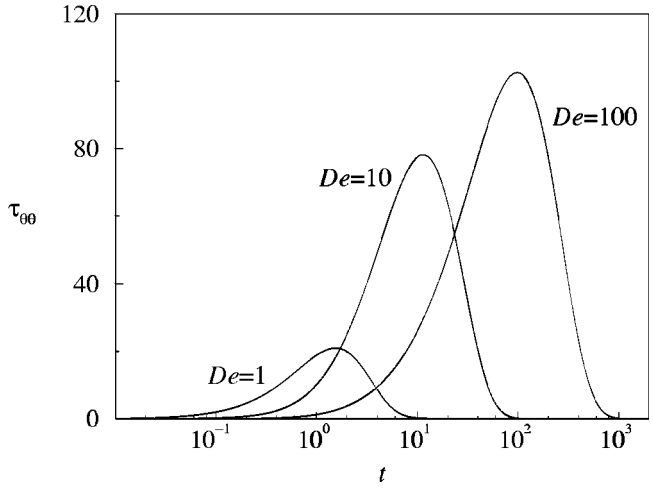

FIG. 7. Evolution of the tensile stress $\tau_{\theta\theta}$ on the bubble surface at different De. Since the same diffusion time scale R_0^2/D is used to construct De and the dimensionless time t, $\tau_{\theta\theta}$ attains a maximum at $t \approx$ De.

magnitude. Thus, the viscoelasticity is manifested mainly by $\tau_{\theta\theta}$. As mentioned before, $\tau_{\theta\theta}$ develops a steep boundary layer at the bubble, and Fig. 7 plots the temporal evolution of $\tau_{\theta\theta}$ at the bubble surface for three different De. A larger De corresponds to a longer relaxation time λ. Thus, $\tau_{\theta\theta}$ grows more slowly after the onset of deformation, but attains a higher maximum value at a time roughly equal to the relaxation time. The crossover in Fig. 6 is simply because the polymer stress takes time to build up (Bousfield *et al.* 1988). A crossover takes place in cell-model calculations as well (Fig. 8) if the shell contains sufficient dissolved gas to sustain bubble growth over a period longer than λ. A similar behavior was reported by Bousfield *et al.* (1986) for the growth of capillary instability on viscoelastic filaments. Previous computations on bubble growth missed it mostly because they were not carried on long enough. Possible inaccuracy due to poor mesh resolution may also have masked the crossover.

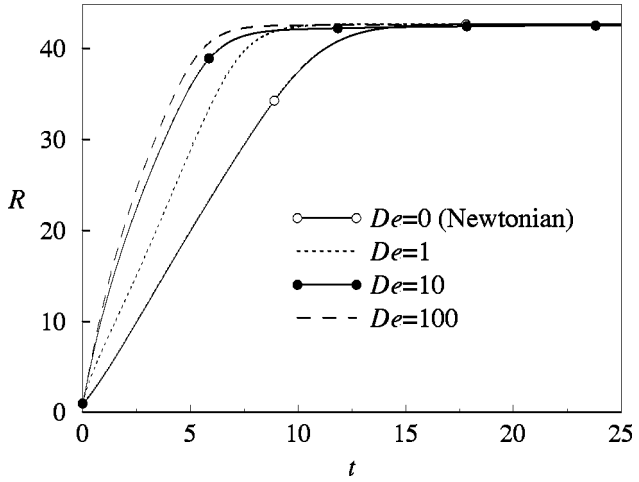

FIG. 8. Effects of De on bubble growth in a shell of Oldroyd-B melt. All other parameters are the same as in Fig. 5.

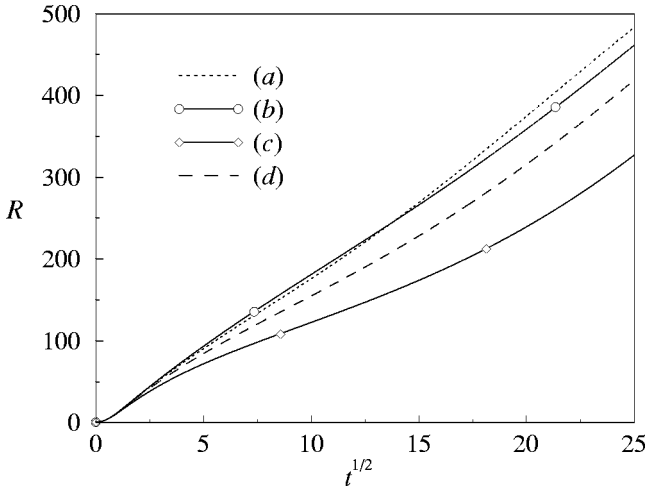

FIG. 9. Effects of the polymer molecular weight M and a high-MW additive on bubble growth in an infinite expanse of melt. (a) De = 100; (b) De = 200; (c) De = 200 with M doubled and the viscosity increased by a factor of $2^{3.4}$; (d) with a second mode added to (a): $\mathrm{De}_2 = 200$, $\beta_2 = 2$. All other parameters are the same as in Fig. 5.

The second issue is the practical relevance of the viscoelastic behavior discussed above. The relaxation time for polymer melts used for foaming is typically on the order of seconds. The process time for extrusion and molding easily exceeds 10 s (Han and Yoo 1981; Ramesh *et al.* 1991). This is long enough for the stiffness of the polymer chains to be felt, and for the crossover to be practically significant. In reality, however, it is impossible to increase the relaxation time of the melt while keeping its viscosity unchanged. With increasing molecular weight M, the viscosity increases as $M^{3.4}$ (Doi and Edwards 1986, p. 237), and would easily overwhelm the initially soft reaction of longer molecules. This is demonstrated in Fig. 9. Curves (a) and (b) differ only in De and a crossover occurs. Curve (c) corresponds to a doubled M; the higher viscosity dampens bubble growth and prevents a crossover with curve (a). The common practice of adding a high-MW additive to increase melt strength (Sandler *et al.* 2000; Azimipour 2002) has a similar effect. This is modeled by including a second Oldroyd-B mode, with a longer relaxation time, in the polymer stress

$$\tau_{rr2}+\mathrm{De}_2\left(\frac{d\tau_{rr2}}{dt}+\frac{4R^2\dot{R}}{r^3}\tau_{rr2}\right) = -4\beta_2\frac{R^2\dot{R}}{r^3}, \tag{40}$$

$$\tau_{\theta\theta2}+\mathrm{De}_2\left(\frac{d\tau_{\theta\theta2}}{dt}-\frac{2R^2\dot{R}}{r^3}r_{\theta\theta2}\right) = 2\beta_2\frac{R^2\dot{R}}{r^3}. \tag{41}$$

With increased viscosity, curve (d) in Fig. 9 shows that the second mode diminishes the rate of bubble growth, as has been documented in experiments (Sandler *et al.* 2000). The longer relaxation time of the second mode does not cause a crossover with curve (a).

IV. CELL SIZE DISTRIBUTION

To predict the final cellular structure of a foam, one needs to integrate the two processes discussed separately in the preceding sections: bubble nucleation and growth. The

only such efforts, as far as we know, have come from Flumerfelt and coworkers (Shafi *et al.*, 1996, 1997; Joshi *et al.* 1998). They used the classical nucleation theory to estimate the nucleation rate, and determined the initial bubble radius $R_0 > R_{cr}$ as the ''upper bound of the critical region'' (Shafi and Flumerfelt 1997). Simultaneous nucleation and growth is modeled by introducing an ''influence volume'' surrounding a bubble inside which the gas concentration is too low for nucleation to occur. Nucleation takes place only in the residue volume, which dwindles in time to zero as the bubbles and their influence volume expand. Regardless of their time of birth, all bubbles have the same initial radius and growth curve, and the final cell size distribution (CSD) is largely a result of different times of nucleation. For Newtonian melts (Shafi *et al.* 1996, 1997), the predicted CSD does not resemble the lognormal shape indicated by experiments (Han and Han 1990a; 1990b; Kieken 2001). In particular, the size distribution function seems to show a minimum for an intermediate bubble size. With a viscoelastic model (Joshi *et al.* 1998), the minimum disappears; the cumulative CSD assumes a smooth tail for smaller bubbles but still ends abruptly for the largest bubbles. No comparison is made with experiments.

We believe that the failure to predict a realistic CSD is due to their nucleation model. First, it is well known that the classic nucleation theory grossly underpredicts the nucleation rate (Saunders 1991), and does not apply to polymer foaming processes where nucleation is dominated by particulate impurities or added nucleating agents. In addition, Shafi and Flumerfelt's (1997) perturbation procedure for deriving the initial conditions for bubble growth is in error. As described in Sec. II, our nucleation model is based on bubble formation from pre-existing microvoids on solid particles, with an initial R_0 determined by the size of the solid particle [Eq. (1)]. But our treatment of simultaneous nucleation and growth, via the primary and secondary bubbles [Eq. (2)], is in fact inspired by the influence volume of Shafi *et al.* (1996).

Since the nucleation rate for secondary bubbles depends on the blowing agent concentration $c_s(t)$ in the vicinity of the nucleating site, and $c_s(t)$ in turn depends on the growth of the primary bubble, we need to compute the growth curves for the primary bubbles. This task has two prerequisites: the initial radius R_0 for the primary bubble, and a means to account for neighboring bubbles competing for the dissolved gas. For the first, an initial size distribution for R_0 can be obtained if the solid particle size distribution is known. For the second, we use the cell model (Amon and Denson 1986; Arefmanesh *et al.* 1990; Koopmans *et al.*, 2000). By assuming that the cells are spherical and uniformly distributed in space, we can determine the amount of melt assigned to each bubble, primary and secondary alike, if the total number of bubbles is known. Thus, both prerequisites require experimental input in the end, a consequence of the phenomenology introduced into Eqs. (1) and (2).

For this purpose, we will use the foam extrusion experiment of Kieken (2001). The polymer is a commercial polystyrene and the blowing agent is a hydrochlorofluorocarbon HCFC-142b. Talc particles of a known size distribution are added as nucleating agents, and the mixture is extruded at temperatures ranging from 130 to 150 °C. The expansion of the foam is recorded as a function of the distance from the die exit. The final bubble number density and size distribution are determined by microscopically examining the solidified foam; the measured CSD will serve as the benchmark for our prediction. The talc particle size distribution (PSD) is well represented by a lognormal distribution, as is usually the case for powders produced by crushing and grinding (Filio *et al.*, 1994)

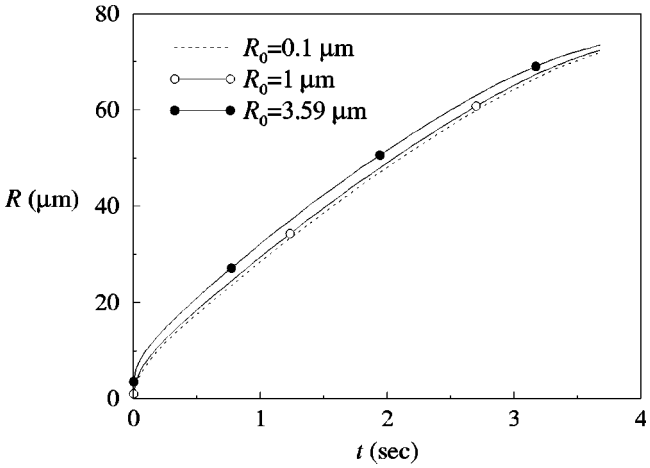

FIG. 10. Growth curves for the primary bubbles computed using the Kieken's (2001) experimental parameters for three R_0 values.

$$\psi_p(R_p) = \frac{1}{\sqrt{2\pi}\sigma R_m^p}\exp\left[-\frac{(\ln R_p - \ln R_m^p)^2}{2\sigma^2}\right], \tag{42}$$

with $R_m^p = 1.028\ \mu$m, $\sigma = 1.094$. The cumulative particulate size distribution is written in terms of the error function

$$Y_p(R_p) = \frac{1}{2}\left[1+\mathrm{erf}\left(\frac{\ln R_p - \ln R_m^p}{\sqrt{2}\sigma}\right)\right]. \tag{43}$$

Using Eq. (1), $\psi_p(R_p)$ and $Y_p(R_p)$ easily translate to an initial size distribution for the primary bubbles

$$\psi_0(R_0) = \frac{1}{\sqrt{2\pi}\sigma R_m}\exp\left[-\frac{(\ln R - \ln R_m)^2}{2\sigma^2}\right], \tag{44}$$

$$Y_0(R_0) = \frac{1}{2}\left[1+\mathrm{erf}\left(\frac{\ln R - \ln R_m}{\sqrt{2}\sigma}\right)\right], \tag{45}$$

where $R_m = \epsilon R_m^p$ [cf. Eq. (1)]. Since only particles larger than a threshold ($R_p > R_{\mathrm{cr}}/\epsilon$) nucleate viable bubbles ($R_0 > R_{\mathrm{cr}}$), the PSD tail for finer particles does not contribute to the foaming process. Thus, ψ_0 and Y_0 differ from the true initial CSD by the small bubbles ($R_0 < R_{\mathrm{cr}}$) that are never nucleated. Thanks to the large disparity between the average particle size and R_{cr} (given below), however, this difference is negligible.

From Kieken's (2001) data on foam expansion and the final bubble number density, we determine the amount of melt for each bubble, which produces an initial radius of the polymer shell $S_0 = 22.43R_0$. The material properties and processing conditions in Kieken (2001) give the following dimensional parameters: $P_0 = 5.24\times10^6$ Pa, $P_a = 1.01\times10^5$ Pa, $\sigma = 0.03$ N/m, $\mu_s = 0$, $\mu_p = 6.61\times10^4$ Pa s, $\rho = 1168.5$ kg/m^3, $k = 2.45\times10^{-5}$ s^2/m^2, $A = 2.93\times10^{-5}$ s^2/m^2, and $\lambda = 1.65$ s.

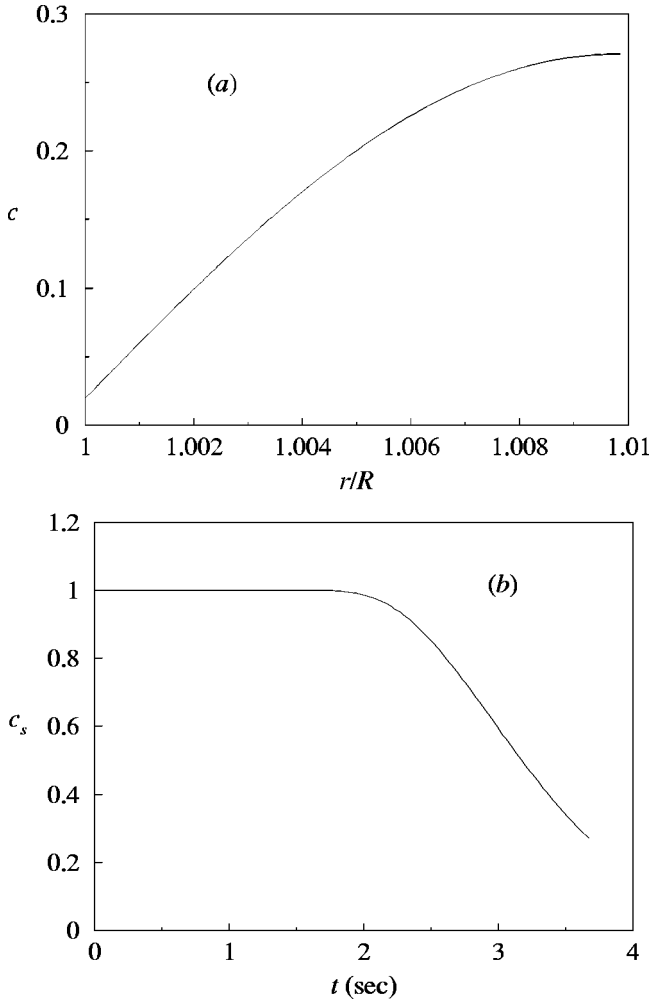

FIG. 11. (a) Gas concentration profile at the end of the run, $t = 3.68$ s and $R = 72.34\ \mu$m, for $R_0 = 1\ \mu$m. (b) Temporal decline of the gas concentration $c_s(t)$ at the outer edge of the shell.

The diffusivity of HCFC-142b in polystyrene is found in Albouy *et al.* (1998): $D = 3 \times 10^{-13}$ m^2/s. Both λ and μ_p reflect the amount of dissolved blowing agent in the resin. The foaming time is $T = 3.68$ s, long enough for the viscoelasticity of the material to be manifested. Under these conditions, the critical bubble radius is $R_{\rm cr} = 1.17 \times 10^{-2}\ \mu$m.

We have chosen some 30 values of R_0, from $R_{\rm cr}$ to several microns, and computed the growth curves $R = R(R_0, t)$ as in Sec. III B. Three examples are shown in Fig. 10. The growth curves generally exhibit two interesting features. First, R is not very sensitive to R_0. R_0 enters the calculation through Eqs. (13) and (15). Since typically $P_a \gg 2\sigma/R_0$, R_0 has only a small effect on $P_g(0)$ and hence $R(t)$. This suggests that a primary bubble cannot dominate the neighborhood of a solid particle as Ramesh *et al.* (1994a) surmised, and that nucleation continues while the primary bubble grows [cf. Eq. (2)]. Second, the bubble growth tends to reach an upper bound towards the end of the simulation, with the effect of narrowing the size distribution of the primary bubbles. This

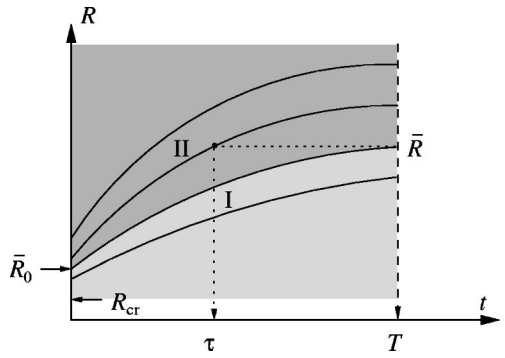

FIG. 12. Schematic showing the procedure for calculating $M(\bar{R})$ using the growth curves.

is evidently because the blowing agent dissolved in the shell is being exhausted. Figure 11 shows a typical gas concentration profile in the shell at the end of the simulation as well as the decline of the gas concentration at the outer edge of the polymer shell.

For determining the nucleation rate of the secondary bubbles, we identify the gas concentration at the outer edge of the polymer shell, plotted in Fig. 11(b), with $c_s(R_0,t)$ in Eq. (2). Now we can calculate the CSD of the foam using the initial size distribution of the primary bubbles $\psi(R_0)$ [Eq. (44)], their growth curves $R(R_0,t)$ (Fig. 10), and the nucleation rate of secondary bubbles $Q(R_0,t)$ [Eq. (2)]. If the total number of solid particles is N_p, then the number of primary bubbles with radius between R_0 and R_0+dR_0 is $N_p\psi(R_0)dR_0$. Over time dt, the number of secondary bubbles produced near these primary bubbles is $(Qdt)N_p\psi(R_0)dR_0$. Thus the total number of bubbles in the final foam is

$$M_{\text{total}} = \int_{R_{\text{cr}}}^{\infty}\left[1+\frac{\gamma D}{R_0^2}\int_0^T c_s(R_0,t)dt\right]N_p\psi(R_0)dR_0$$

$$= N_p[1-Y_0(R_{\text{cr}})]+N_p\gamma D\int_{R_{\text{cr}}}^{\infty}\left(\int_0^T c_s(R_0,t)dt\right)\frac{\psi(R_0)}{R_0^2}dR_0, \qquad (46)$$

with the two terms representing the number of primary and secondary bubbles, respectively. Note that $\psi(R_0)$ depends on the phenomenological constant ϵ via R_m. We have tested several values of ϵ in the range of 0.1 to 0.5. For each, we equate M_{total} to the *measured* total number of cells to determine the growth rate constant γ. Results show that γ increases with ϵ from roughly 0.01 to 0.1. This is easily understandable since a larger ϵ activates smaller particles for nucleation. This shifts the most productive particles with R_p just above R_{cr}/ϵ, toward the tail of the PSD. With the number of most productive particles diminished, a larger γ is required to produce the same number of secondary bubbles. With ϵ increasing from 0.1 to 0.5, the fraction of small inviable bubbles neglected in Eqs. (44) and (45) drops from 2.3 to 0.027%.

Using the γ value for each ϵ, we calculate the number of bubbles $M(\bar{R})$ below a certain radius $\bar{R}$. Then the cumulative CSD of the foam is simply

$$Y(\bar{R}) = M(\bar{R})/M_{\text{total}}. \qquad (47)$$

Figure 12 illustrates the bubble growth curves from a range of initial radii. Let $\bar{R}$ corre-

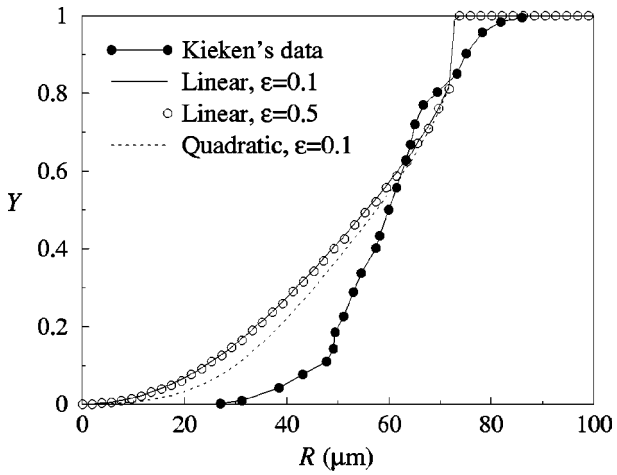

FIG. 13. Comparison between the cumulative CSD measured by Kieken (2001) and our model predictions using $\epsilon = 0.1$ and 0.5. "Linear" refers to the nucleation rate in Eq. (2) whereas "quadratic" refers to Eq. (50).

spond to a primary bubble with an initial radius $\bar{R}_0$: $\bar{R} = R(\bar{R}_0, T)$. Bubbles smaller than $\bar{R}$ at the end of foaming fall into two groups: (I) those that have originated from an initial radius $R_0 < \bar{R}_0$, and (II) those that have an initial radius $R_0 > \bar{R}_0$ but have been born late. The first group, indicated by the lighter area in Fig. 12, consists of primary bubbles, which have grown for the entire time T, and secondary bubbles that are nucleated after the inception of foaming and thus have grown for shorter periods of time. The total number of bubbles in group I can be calculated in a similar fashion to Eq. (46)

$$M_{\mathrm{I}} = \int_{R_{\mathrm{cr}}}^{\bar{R}_0}\left[1+\frac{\gamma D}{R_0^2}\int_0^T c_s(R_0,t)\,dt\right]N_p\psi(R_0)\,dR_0$$

$$= N_p[Y_0(\bar{R}_0)-Y_0(R_{\mathrm{cr}})]+N_p\gamma D\int_{R_{\mathrm{cr}}}^{\bar{R}_0}\left(\int_0^T c_s(R_0,t)\,dt\right)\frac{\psi(R_0)}{R_0^2}\,dR_0. \qquad (48)$$

Group II contains secondary bubbles only since a primary bubble starting from an initial radius $R_0 > \bar{R}_0$ will have grown beyond $\bar{R}$ at $t = T$, and thus will not be counted in $M(\bar{R})$. Furthermore, these secondary bubbles have to be so young that they have not had time to grow beyond the radius $\bar{R}$ by the end of foaming. More specifically, for each growth curve originating from an initial radius $R_0 > \bar{R}_0$, we can find a time $\tau < T$ such that $\bar{R} = R(R_0, \tau)$ (cf. Fig. 12). Then the secondary bubbles with initial radius R_0 and final radius $R < \bar{R}$ must not have grown for longer than τ. In other words, they must have nucleated in the interval $T-\tau \leqslant t \leqslant T$. Thus, the number of bubbles in group II can be calculated as

$$M_{\mathrm{II}} = N_p\gamma D\int_{\bar{R}_0}^{\infty}\left(\int_{T-\tau(R_0)}^{T} c_s(R_0,t)\,dt\right)\frac{\psi(R_0)}{R_0^2}\,dR_0. \qquad (49)$$

The total number of bubbles below $\bar{R}$ at the end is $M(\bar{R}) = M_{\mathrm{I}}+M_{\mathrm{II}}$.

Using the above procedure, the cumulative cell size distribution is calculated, and Fig. 13 compares those for two ϵ values with the measured cumulative CSD at $t = 3.68$ s.

The predicted distributions present a few interesting features. First, the median bubble radius agrees with the measurement to remarkable accuracy; the experimental value $R_m = 60\ \mu$m is only about 8% larger than the predictions $R_m = 55.3–56.4\ \mu$m. The only ''free parameter'' of the model is ϵ, the ratio between the size of an initial bubble and the particle that has produced it. For the same nucleating particles, a larger ϵ increases the initial and thus the final bubble size. But increasing ϵ from 0.1 to 0.5, a reasonable range considering the probable size of cavities on the particle (cf. Fig. 1), has only a very weak effect on $Y(R)$; it shifts the lower portion of the CSD slightly toward larger R. This is because R is relatively insensitive to the initial radius as noted before. Thus our theory predicts the median bubble size to within 8% essentially without the help of fitting parameters. Considering the large number of parameters and the complexity of the experimental conditions, this degree of agreement is perhaps fortuitous. For instance, the rheology of the gas-containing melt depends on the gas concentration c and the temperature. Both experience large variations in the actual extrusion, which are not accounted for in the constitutive model.

The second feature is that the theoretical Y curves have two distinct parts. The gently sloped lower portion $Y < 0.8$ is due mainly to the nucleation of secondary bubbles, whereas the steep upper portion is due to the growth of the primary bubbles. As compared with the experimental CSD, the predicted size distribution is too wide in the lower portion but too narrow in the upper portion. The prevalence of small secondary bubbles in the CSD is a result of late nucleations. Whereas our nucleation rate in Eq. (2) declines *linearly* with c_s [cf. Fig. 11(b)], nucleation drops off more drastically in the experiment once bubble growth is underway. The linear model is based on considerations of bubble growth before detachment. In dimensionless terms, the far-field concentration c_0 enters k^* [Eq. (35)], which affects the bubble mass balance [Eq. (19)] and the boundary condition for gas concentration outside the bubble [Eq. (24)]. From Eq. (19), one reasons that the time needed for a bubble to gain a certain mass scales inversely with c_0. Thus Q is made linearly proportional to c_s in Eq. (2). The fact that this linear relationship underestimates the suppression of nucleation by a declining c_s is not entirely surprising since k^* also affects $\partial c/\partial r|_{r=R}$ in Eq. (19) via the boundary condition in Eq. (24). A lower c_s or larger k^* raises the gas concentration outside the bubble for the same bubble pressure, and thus reduces $\partial c/\partial r$ and the mass diffusion into the bubble. This can be a considerable effect, but it is not obvious how to model it. We have tested a nucleation rate with a *quadratic* dependence on c_s:

$$Q = \gamma \frac{D c_s^2}{R_0^2}. \tag{50}$$

This indeed narrows the lower portion of the CSD in Fig. 13 and brings it closer to the experimental curve. One must note that the distinction of primary and second bubbles is somewhat artificial, and Q depends on the collective effect of *all bubbles* that are consuming the blowing agent in the neighborhood. Thus, Eq. (50) demonstrates the correct trend but is far from a perfect model; a more rational approach to the $Q \sim c_s$ relationship is needed.

Toward the other end of the CSD, the narrow distribution for the primary bubbles is directly related to the upper bound for $R(t)$ in Fig. 10, and is therefore a consequence of the cell model. It is not clear how well this upper bound represents reality, where bubbles deform into polyhedra separated by a network of polymer films. Furthermore, bubble coalescence may have occurred in the later stage of foaming in the experiment, causing the CSD to broaden for the largest bubbles.

V. CONCLUSION

In this study, we aim to accomplish three tasks, which, along with their respective outcome, are summarized below.

(i) To formulate a nucleation model that highlights the role of nucleating agents. We combine elements of the Ramesh *et al.* (1994a) nucleation model and classical boiling theory to form a picture of pre-existing microbubbles growing and detaching from solid particles. Continuous nucleation is modeled by assuming a detachment time that scales with the diffusion time. The effect of decreasing gas concentration on the nucleation rate is also incorporated.

(ii) To clarify the role of viscoelasticity in bubble growth in a polymer melt. If the process time is shorter than the relaxation time of the polymer, melt strength is not fully exhibited and this has led previous researchers to conclude that viscoelasticity enhances bubbles growth. In typical foam molding and extrusion operations, however, the process time is long enough for the polymer chains to be substantially extended. Then the elevated elongational viscosity tends to suppress bubble growth. The well-known effect of high molecular-weight additives to produce smaller bubbles, however, has to do with an increased zero-deformation viscosity rather than viscoelasticity.

(iii) To integrate bubble nucleation and growth and predict the final cell size distribution. The predictions are in reasonably good agreement with experimental measurement. The prevalence of small bubbles in the theoretical CSD suggests that our nucleation model under-estimates the effect of older bubbles to inhibit further nucleation. On the other hand, the larger bubbles have too narrow a distribution, probably due to the lack of coalescence in the model.

We close by emphasizing the limitations of this work. The treatment of simultaneous nucleation and growth via the concept of primary and secondary bubbles needs to be improved so the two factors merge into each other more smoothly than in Fig. 13. Underlying this inadequacy are the limitations of the cell model. By reserving a fixed amount of virgin melt for each primary and secondary bubble, the cell model assumes that a bubble's growth is determined by its immediate neighborhood and the melt farther out remains saturated until a bubble nucleates there. In reality, however, younger bubbles will have a smaller supply of dissolved gas. Thus, our using the same growth curve for all bubbles is self-consistent within the cell model but may not reflect reality. Making the nucleation rate Q depend on the gas concentration c_s [Eqs. (2) and (50)] in fact breaks away from the cell picture. A fundamental resolution of these issues calls for a direct simulation of a multibubble system with simultaneous nucleation and growth.

The Oldroyd-B model is only a qualitative representation of the melt viscoelasticity during biaxial extension (Khan and Larson 1987). Furthermore, it does not reflect evolving degrees of plasticization and a changing temperature in real processes, both influential determinants of the melt rheology. Geometrically, the modeling is restricted to a single spherical bubble. Thus, bubble-bubble interactions, including deformation and coalescence, are not properly accounted for. Finally, spatial homogeneity is assumed so the macro-scopic spatial variations in pressure, temperature, flow velocity, and bubble distribution are not considered (Arefmanesh *et al.* 1990; Koopmans *et al.* 2000). These issues present an interesting array of opportunities for future work.

ACKNOWLEDGMENTS

This work was supported by an NSF Career Award and a grant from ATOFINA Chemicals, Inc. The authors acknowledge helpful discussions with Professor D. C. Venerus of Illinois Institute of Technology, Professor I. Kusaka of Ohio State University,

Professor Chun Liu of Pennsylvania State University, and Doctor J. Wu, Doctor B. Azimipour, and Doctor G. O'Brein of ATOFINA Chemicals, Inc.

References

Albouy, A., J.-D. Roux, D. Mouton, and J. Wu, ''Development of HFC blowing agents. Part II: Expanded polystyrene insulating boards,'' Cellular Polym. **17**, 163–176 (1998).

Amon, M., and C. D. Denson, ''A study of the dynamics of foam growth: analysis of the growth of closely spaced spherical bubbles,'' Polym. Eng. Sci. **24**, 1026–1034 (1984).

Amon, M., and C. D. Denson, ''A study of the dynamics of foam growth: Simplified analysis and experimental results for bulk density in structural foam molding,'' Polym. Eng. Sci. **26**, 255–267 (1986).

Arefmanesh, A., and S. G. Advani, ''Diffusion-induced growth of a gas bubble in a viscoelastic fluid,'' Rheol. Acta **30**, 274–283 (1991).

Arefmanesh, A., S. G. Advani, and E. E. Michaelides, ''A numerical study of bubble growth during low pressure structural foam molding process,'' Polym. Eng. Sci. **30**, 1330–1337 (1990).

Azimipour, B., ''Process aid for cellular PVC,'' Technical Report, ATOFINA Chemicals Inc. (personal communication, 2002).

Blander, M., and J. L. Katz, ''Bubble nucleation in liquids,'' AIChE J. **21**, 833–848 (1975).

Bousfield, D. W., R. Keunings, and M. M. Denn, ''Transient deformation of an inviscid inclusion in a viscoelastic extensional flow,'' J. Non-Newtonian Fluid Mech. **27**, 205–221 (1988).

Bousfield, D. W., R. Keunings, G. Marrucci, and M. M. Denn, ''Nonlinear analysis of the surface tension driven breakup of viscoelastic filaments,'' J. Non-Newtonian Fluid Mech. **21**, 79–97 (1986).

Chen, L., X. Wang, R. Straff, and K. Blizard, ''Shear stress nucleation in microcellular foaming process,'' Polym. Eng. Sci. **42**, 1151–1158 (2002).

Cole, R., ''Boiling nucleation,'' Adv. Heat Transfer **10**, 85–166 (1974).

Colton, J. S., and N. P. Suh, ''The nucleation of microcellular thermoplastic foam with additives: Part I: Theoretical considerations,'' Polym. Eng. Sci. **27**, 485–492 (1987).

Doi, M. and S. F. Edwards, *The Theory of Polymer Dynamics* (Oxford University Press, New York 1986).

Duda, J. L., and J. S. Vrentas, ''Mathematical analysis of bubble dissolution,'' AIChE J. **15**, 351–356 (1969).

Filio, J. M., K. Sugiyama, F. Saito, and Y. Waseda, ''A study on talc ground by tumbling and planetary ball mills,'' Powder Technol. **78**, 121–127 (1994).

Griffith, P., and J. D. Wallis, ''The role of surface conditions in nucleate boiling,'' Chem. Eng. Prog., Symp. Ser. **56**(30), 49–63 (1960).

Guo, M. C., and Y. C. Peng, ''Study of shear nucleation theory in continuous microcellular foam extrusion,'' Polym. Test. **22**, 705–709 (2003).

Han, C. D., and H. J. Yoo, ''Studies on structural foam processing. Part IV: Bubble growth during molding filling,'' Polym. Eng. Sci. **21**, 518–533 (1981).

Han, J. H., and C. D. Han, ''Bubble nucleation in polymeric liquids. Part I: Bubble nucleation in concentrated polymer solutions,'' J. Polym. Sci., Part B: Polym. Phys. **28**, 711–741 (1990a).

Han, J. H., and C. D. Han, ''Bubble nucleation in polymeric liquids. Part II: Theoretical considerations,'' J. Polym. Sci., Part B: Polym. Phys. **28**, 743–761 (1990b).

Hodgson, A. W., ''Homogeneous nucleation,'' Adv. Colloid Interface Sci. **21**, 303–327 (1984).

Joshi, K., J. G. Lee, M. A. Shafi, and R. W. Flumerfelt, ''Prediction of cellular structure in free expansion of viscoelastic media,'' J. Appl. Polym. Sci. **67**, 1353–1368 (1998).

Khan, S. A., and R. G. Larson, ''Comparison of simple constitutive equations for polymer melts in shear and biaxial and uniaxial extensions,'' J. Rheol. **31**, 207–234 (1987).

Kieken, B., ''Processing and performance of PS foamed with HCFC-142b and HFC-134a,'' Technical Report, ATOFINA Chemicals, Inc. (personal communication 2001).

Koopmans, R. J., J. C. F. den Doelder, and A. N. Paquet, ''Modeling foam growth in thermoplastics,'' Adv. Mater. (Weinheim, Ger.) **12**, 1873–1880 (2000).

Lee, S.-T., *Foam Extrusion*, (Technomic, Lancaster, PA, 2000).

Lee, J. G., and R. W. Flumerfelt, ''A refined approach to bubble nucleation and polymer foaming process: dissolved gas and cluster size effects,'' J. Colloid Interface Sci. **184**, 335–348 (1996).

Park, C. B., L. K. Cheung, and S. W. Song, ''The effect of talc on cell nucleation in extrusion foam processing of polypropylene with CO_2 and isopentane,'' Cellular Polym. **17**, 221–251 (1998).

Press, W. H., S. A. Teukolsky, W. T. Vetterling, and B. P. Flannery, *Numerical Recipes in Fortran 77*, 2nd ed. (Cambridge University Press, New York, 1992).

Ramesh, N. S., D. H. Rasmussen, and G. A. Campbell, ''Numerical and experimental studies of bubble growth during the microcellular foaming process,'' Polym. Eng. Sci. **31**, 1657–1664 (1991).

Ramesh, N. S., D. H. Rasmussen, and G. A. Campbell, ''The heterogeneous nucleation of microcellular foams assisted by the survival of microvoids in polymers containing low glass transition particles. Part I: Mathematical modeling and numerical simulation,'' Polym. Eng. Sci. **34**, 1685–1697 (1994a).

Ramesh, N. S., D. H. Rasmussen, and G. A. Campbell, ''The heterogeneous nucleation of microcellular foams assisted by the survival of microvoids in polymers containing low glass transition particles. Part II: Experimental results and discussion,'' Polym. Eng. Sci. **34**, 1698–1706 (1994b).

Sandler, J., F. Wöllecke, V. Altsädt, E. Wettstein, and D. Rakutt, ''Principal correlation of PVC melt elongational properties with foam cell morphology,'' Cellular Polym. **19**, 371–388 (2000).

Saunders, J. H., ''Fundamentals of foam formation,'' in *Handbook of Polymeric Foams and Foam Technology*, D. Klempner and K. C. Frisch eds., (Hanser Publishers, New York, 1991), Chap. 2.

Shafi, M. A., and R. W. Flumerfelt, ''Initial bubble growth in polymer foam processes,'' Chem. Eng. Sci. **52**, 627–633 (1997).

Shafi, M. A., K. Joshi, and R. W. Flumerfelt, ''Bubble size distribution in freely expanded polymer foams,'' Chem. Eng. Sci. **52**, 635–644 (1997).

Shafi, M. A., J. G. Lee, and R. W. Flumerfelt, ''Prediction of cellular structure in free expansion polymer foam processing,'' Polym. Eng. Sci. **36**, 1950–1959 (1996).

Street, J. R., ''The rheology of phase growth in elastic liquids,'' Trans. Soc. Rheol. **12**, 103–131 (1968).

Tatibouët, J., R. Gendron, A. Hamel, and A. Sahnoune, ''Effect of different nucleating agents on the degassing conditions as measured by ultrasonic sensors,'' J. Cell. Plast. **38**, 203–218 (2002).

Venerus, D. C., and N. Yala, ''Transport analysis of diffusion-induced bubble growth and collapse in viscous liquids,'' AIChE J. **43**, 2948–2959 (1997).

Venerus, D. C., N. Yala, and B. Bernstein, ''Analysis of diffusion-induced bubble growth in viscoelastic liquids,'' J. Non-Newtonian Fluid Mech. **75**, 55–75 (1998).

Yarin, A. L., D. Lastochkin, Y. Talmon, and Z. Tadmor, ''Bubble nucleation during devolatization of polymer melts,'' AIChE J. **45**, 2590–2605 (1999).